

Article

Catalytic Activity of Mixed Al₂O₃-ZrO₂ Oxides for Glucose Conversion into 5-Hydroxymethylfurfural

Benjamín Torres-Olea, Sandra Mérida-Morales, Cristina García-Sancho * ,
Juan Antonio Cecilia  and Pedro Maireles-Torres 

Departamento de Química Inorgánica, Cristalografía y Mineralogía (Unidad Asociada al ICP-CSIC),
Facultad de Ciencias, Campus de Teatinos, Universidad de Málaga, 29071 Málaga, Spain;
benjamin@uma.es (B.T.-O.); sandra_merida@uma.es (S.M.-M.); jacecilia@uma.es (J.A.C.);
maireles@uma.es (P.M.-T.)

* Correspondence: cristinags@uma.es; Tel.: +34-951-953-298

Received: 20 July 2020; Accepted: 31 July 2020; Published: 4 August 2020



Abstract: In the present work, a series of catalysts based on aluminum and zirconium oxides was studied for the transformation of glucose into 5-hydroxymethylfurfural. These catalysts were characterized by using experimental techniques, such as X-ray diffraction, N₂ adsorption–desorption at –196 °C, X-ray photoelectron spectroscopy, temperature-programmed desorption of NH₃ and CO₂, and scanning transmission electron microscopy. The catalytic behavior in glucose dehydration was evaluated in a water-methyl isobutyl ketone biphasic system, in the presence of CaCl₂, in order to minimize losses due to unwanted secondary reactions. High glucose conversion and 5-hydroxymethylfurfural (HMF) yield values were obtained in the presence of an Al(Zr)O_x catalyst with an Al:Zr molar ratio of 7:3, reaching 97% and 47%, respectively, at 150 °C after 120 min. Under tested conditions, this catalyst retained most of its catalytic activity for four reuses.

Keywords: glucose; 5-hydroxymethylfurfural; lignocellulosic biomass; heterogeneous catalysts; aluminum oxide; zirconium oxide

1. Introduction

Fossil fuel depletion and ever increasing environmental concerns have prompted scientists' efforts to look for alternative renewable sources for their use as raw material to produce chemicals and fuels [1–3]. In recent years, valorization of biomass wastes has received great attention as an opportunity to reduce our dependency of fossil fuels and replace them with carbon neutral bioresources, because it is a renewable and promising long-term resource [4]. Lignocellulose is the most abundant and more readily accessible biomass source worldwide, in which cellulose polymers are packed within hemicellulose foil and connected to each other by lignin [5]. Its composition varies among different types of biomass, in such a way that cellulose is frequently around 50%, lignin about 20%, and hemicellulose shows more variability [6]. Therefore, cellulose is usually the most abundant compound in lignocellulosic biomass, which is a crystalline polysaccharide composed of glucose units linked through beta-1,4-D-glycosidic bonds [6].

5-hydroxymethylfurfural (HMF) is a platform molecule, which can be obtained through dehydration of hexoses in the presence of acid catalysts, and it can be employed as precursor for polymer synthesis [7], biofuels [8–10] and other bulk chemicals, as levulinic and formic acids among others [11]. In the literature, fructose, coming from glucose isomerization, has been efficiently dehydrated to HMF. Thus, Shimizu et al. [12] attained HMF yield values of 100% by using an ion-exchange resin, Amberlyst-15, as an acid catalyst. Despite high yields have been obtained from fructose, high costs of its enzymatic production process [13] are hindering the scale-up production of

HMF to sustain biofuel [9,14] and polymer industries [15]. In this context, glucose appears abundantly in nature and can also be chemically transformed to HMF. As aforementioned, cellulose is formed by glucose units, which can be obtained by hydrolysis. Thus, competitive methods of glucose dehydration to HMF are being actively evaluated, since the use of glucose as starting material is more interesting because it is cheap, widely available and can be obtained from cellulose fraction of lignocellulosic biomass [5].

Unlike fructose, the transformation of glucose into HMF displays some important drawbacks, since this takes place through consecutive reactions (isomerization and subsequent dehydration), in such a way that it is required the development of economical, efficient and environmentally friendly catalytic processes. Most of them employed water as the solvent, as cellulose hydrolysis is accomplished in water, but HMF is unstable in acidic aqueous conditions, since it undergoes side-reactions, such as auto-condensation and resinification, considerably reducing its yield [16,17]. To mitigate such negative effects, organic–water biphasic systems have been reported in the literature, being the most common the use of co-solvents, such as 2-butanol [18,19], tetrahydrofuran [20], cyclopentyl methyl ether [21], and methyl isobutyl ketone (MIBK) [18,22–25]. Thus, most of the HMF is extracted to the organic phase according to the partition coefficient, minimizing the formation of by-products, which takes place mainly in aqueous solution. On the other hand, the addition of alkaline earth salts in the reaction medium has demonstrated to increase glucose conversion and HMF yield, as a consequence of changing partition coefficient [26] and/or promoting favorable reaction pathways through the formation of complexes [22,27]. Thus, the presence of these cations can shift the anomeric equilibrium of glucose towards the predominant α -anomer [28]. In particular, Palagi et al. [27] discovered that calcium cation interacts with C6 hydroxyl and hemiketal oxygens and estimated a complex formation constant with the α -form of $1.5 \text{ L}\cdot\text{mol}^{-1}$. In addition, Garcia Sancho et al. studied the effect of calcium chloride on glucose dehydration to HMF, demonstrating by ^1H NMR spectroscopy that this cation favored the formation of α -anomer and considerably enhanced the HMF production [22].

In order to convert glucose to HMF in a satisfactory way, solid acid catalysts must be employed, which should be able to catalyze the glucose isomerization to fructose and its subsequent dehydration to HMF [13,29]. Glucose isomerization requires Lewis acid or basic sites, while fructose dehydration takes place in the presence of Brønsted acid sites [30–32]. Regarding the glucose isomerization to fructose, which is the limiting step for large scale HMF production, basic catalysts such as hydrotalcites [33–35], cation-exchanged zeolites [33] and alkylamines [36,37] were studied, showing very high selectivity, but a low glucose conversion for isomerization reaction, thus providing low fructose yields. More recently, Lewis acid catalysts have also been utilized with interesting results by using a zirconsilicate [38] or a tin beta-zeolite [39]. However, it is more economically attractive to carry out the HMF production in one-pot process, being necessary a catalyst with both Brønsted and Lewis acid sites able to accomplish directly both steps. Hence, metal oxides have also been studied, such as metal oxides and modified metal oxides of chromium [30,40], niobium [41], titanium [42], zirconium [42,43], aluminum [22,44] or tantalum [19], metal phosphates [20,32], doped silicas [25], and zeolites [45], among others. Concretely, zirconium oxide has been studied as solid acid catalyst for HMF production by itself [46], supported [47] and mixed with other oxides such as TiO_2 [48], Nb_2O_5 [49], SnO_2 [50], and MoO_3 [51]. Thus, Zhang et al. [46] evaluated the influence of calcination temperature for ZrO_2 , attaining total glucose conversion with a selectivity of HMF about 40%. Moreover, ZrO_2 has been frequently deposited over ordered mesoporous structures to increase surface area and improve reactant and product diffusion [52–54]. Likewise, aluminum oxides have been employed to dope mesoporous solids, increasing their acidity for its use as both catalyst and support. Its different phases (boehmite, gibbsite and corundum) [55], together with possibilities of bulk and surface modifications, combined with its high availability and low cost, make aluminum oxides attractive as catalyst in the chemical industry. Moreover, $\gamma\text{-Al}_2\text{O}_3$ provided, after addition of CaCl_2 , relevant catalytic results in a biphasic water:MIBK system, attaining glucose conversion and HMF yield of 96% and 52%, respectively, at $175 \text{ }^\circ\text{C}$ after 15 min [22].

Therefore, mixed aluminum-zirconium oxides, with suitable textural and acidic properties, could be a suitable alternative for the acid-catalyzed dehydration of glucose into HMF. In this work, a series of mixed Al-Zr oxides, with different Al:Zr molar ratio, was prepared and tested for the dehydration of glucose, by using a water: MIBK reaction medium. Their physicochemical properties were determined by different techniques in order to establish the corresponding structure–catalytic performance relationships. In addition, it would be relevant to know if mixed AlZrO_x oxides were more active than the pertinent pure oxides and demonstrate possible interaction between both elements in mixed metal oxides. The influence of different reaction parameters, such as reaction time and temperature, catalyst and glucose loadings, the effect of CaCl_2 and the reuse of catalysts were also evaluated.

2. Results and Discussion

2.1. Catalyst Characterization

Powder X-ray diffraction (XRD) was used to identify crystalline phases present in these catalysts, and it revealed that they were mostly amorphous, or with low crystallinity (Figure 1), mainly when zirconium content increased. In the case of Al catalyst, diffraction peaks at 2θ ($^\circ$) = 14.5, 28.2, 38.3, 48.9, and 64.0 demonstrated the existence of a boehmite phase (AlOOH) (PDF 00-005-0190). However, zirconium-containing catalysts only exhibited a broad band around 30° , which could be associated to very low crystalline zirconia, but it could not be ascribed to monoclinic, tetragonal, or cubic zirconia.

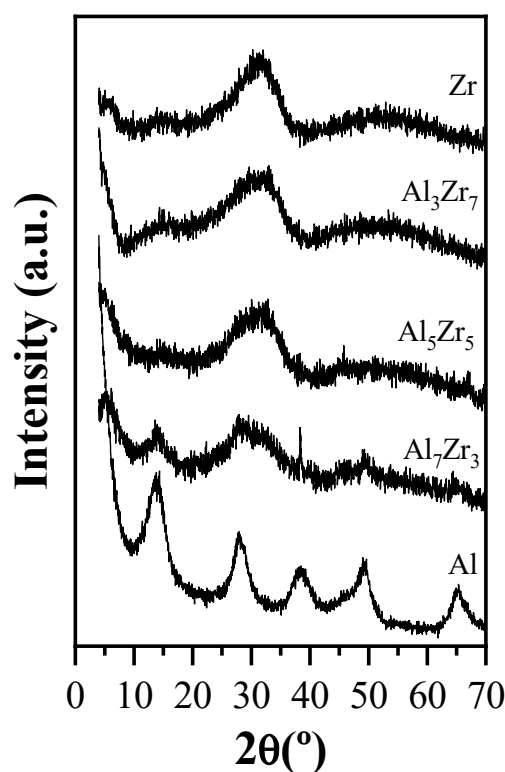


Figure 1. Powder X-ray diffraction (XRD) patterns of Al, Zr, and Al_xZr_y catalysts.

Textural properties were deduced from N_2 adsorption–desorption isotherms (Figure 2A) at -196°C . The Al catalyst exhibits a Type IV isotherm, which is typical of mesoporous materials, with a hysteresis loop of Type H2(a) associated with complex pore structures [56]. However, the adsorption–desorption isotherms tend to be Type I after the incorporation of zirconium to catalysts, which is characteristic of microporous solids. The loss of the hysteresis loop for the Zr-rich catalysts would confirm the increase in microporosity. The textural properties are summarized in Table 1.

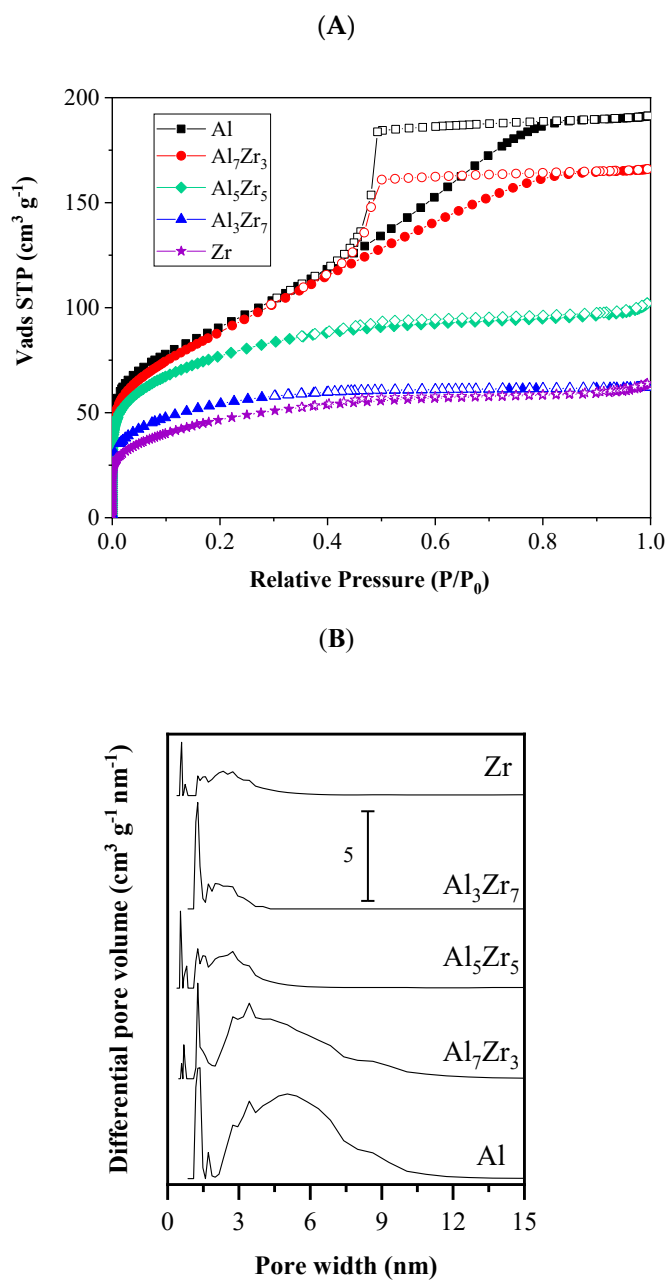


Figure 2. (A) N_2 adsorption–desorption isotherms at $-196\text{ }^\circ\text{C}$ and (B) pore size distributions of Al, Zr, and Al_xZr_y catalysts.

Table 1. Textural and acid–base properties of catalysts.

Catalyst	S_{BET} ($\text{m}^2\cdot\text{g}^{-1}$)	S_{micro} ($\text{m}^2\cdot\text{g}^{-1}$)	V_p ($\text{cm}^3\cdot\text{g}^{-1}$)	V_{micro} ($\text{cm}^3\cdot\text{g}^{-1}$)	μmol $\text{NH}_3\cdot\text{g}_{\text{cat}}^{-1}$	μmol $\text{NH}_3\cdot\text{m}^{-2}$	μmol $\text{CO}_2\cdot\text{g}_{\text{cat}}^{-1}$	μmol $\text{CO}_2\cdot\text{m}^{-2}$
Al	325	5	0.30	0.00	279	0.86	70	0.21
Al_7Zr_3	321	84	0.26	0.04	188	0.59	46	0.14
Al_5Zr_5	274	227	0.15	0.11	270	0.98	67	0.24
Al_3Zr_7	263	248	0.10	0.08	185	0.70	40	0.15
Zr	168	135	0.09	0.06	82	0.49	27	0.16

Both surface area and pore volume gradually decreased from 325 to 168 $\text{m}^2\cdot\text{g}^{-1}$ and 0.30 to 0.09 $\text{cm}^3\cdot\text{g}^{-1}$, respectively, when the Zr content of catalysts increased, being the smallest values found

for the Zr catalyst. However, the presence of zirconium generated a higher amount of micropores, in such a way that both microporous surface area and micropore volume rose, being maximum for the Al_5Zr_5 catalyst. Regarding pore size distribution (Figure 2B), it can be noted that all catalysts exhibited micro- and mesopores. A heterogeneous pore size distribution was found for the Al catalyst, with pore sizes between 1 and 12 nm. This fact was also observed for the Al_7Zr_3 catalyst. However, the incorporation of a higher amount of zirconium led to the formation of pores smaller than 1 nm. Therefore, it could be affirmed that the presence of zirconium affected to microporosity of these catalysts, generating smaller pores than those obtained for Al-rich catalysts.

On the other hand, STEM images evidenced the formation of aggregates and EDX analysis showed that both aluminum and zirconium species were homogeneously dispersed in the catalyst structure (Figure 3).

On the other hand, binding energies (BE) for different elements were compiled in Table 2. In the case of C 1s core level spectra, two contributions can be observed about 284.7–284.9 and 288.4–289.0 eV, which correspond to adventitious carbon and carbonate species, respectively (Figure 4A) [57]. It should be noted that the atomic concentration of C associated to carbonates was very similar in all cases (1.3–2.5%). Likewise, two contributions were found in the O 1s core level spectra, about 529.8–530.1 and 531.6–531.9 eV (Figure 4B). The former corresponds to oxide ions and the latter can be attributed to both hydroxyl groups and oxygen in carbonates. [58–61] Considering that the C atomic concentration for carbonates almost remained unchanged, the decrease of this contribution at 531.7 eV after Zr incorporation could be due to hydroxyl species also decreased. Thus, the Al catalyst showed a higher amount of hydroxyl groups due to the presence of boehmite (AlOOH), as was inferred from XRD, but the band associated to oxide species gained considerable importance over the hydroxyl one with increasing amounts of zirconium (Table 2). Regarding Al $2p_{3/2}$ core level spectra, the Al catalyst only showed a contribution at 73.7 eV (Figure 4C), similar to data previously reported for boehmite in bibliography (73.9 eV) [59], which is in agreement with XRD data confirming the presence of boehmite. This contribution was also found for mixed Al_xZr_y catalysts, although it was shifted to higher BE values in the case of Al_5Zr_5 . In this latter case, a value of 74.1 eV was found, similar to that previously attributed by Klopogge et al. [59] to Al in pseudoboehmite, in which the amount of hydroxyl groups was slightly higher than in boehmite. However, similar BE values have been found for aluminum oxides, being complicated to distinguish between oxides, hydroxides and oxohydroxides by XPS. Therefore, it could be thought that this band corresponds to Al in boehmite in the case of Al catalyst, since this phase was confirmed by XRD. However, in the case of mixed metal oxides, with no crystalline phases detected by XRD, both oxides and oxohydroxides could be responsible of this band. This slight increase in BE for Al 2p in the case of Al_5Zr_5 could also be due to aluminum was strongly interacting with zirconium, as observed Reddy et al. [62]. With respect to the Zr $3d_{5/2}$ core level, a contribution about 181.6–182.1 eV was found (Figure 4D), which is in agreement with data reported in the literature for ZrO_2 [48,60].

Table 2. Atomic ratios and binding energies found in XPS analysis for Al, Zr, and Al_xZr_y catalysts.

Catalyst	Binding Energy (eV) (Atomic Concentration (%))					Atomic Ratio by XPS		Nominal Atomic Ratio	
	C 1s		O 1s	Al 2p	Zr $3d_{5/2}$	Al/Zr	O/(Al + Zr)	Al/Zr	
Al	284.9 (3.8)	288.5 (1.3)	530.1 (30.3)	531.7 (33.3)	73.7 (31.3)	-	-	2.03	-
Al_7Zr_3	284.7 (5.5)	288.4 (1.5)	530.0 (37.4)	531.7 (24.9)	73.7 (24.2)	181.6 (6.4)	3.78	2.04	2.33
Al_5Zr_5	284.8 (9.3)	288.7 (1.8)	529.8 (33.5)	531.8 (25.2)	74.1 (19.0)	181.7 (11.3)	1.68	1.94	1.0
Al_3Zr_7	284.7 (15.6)	289.0 (1.7)	530.0 (42.3)	531.9 (13.8)	73.8 (6.5)	182.1 (20.1)	0.32	2.11	0.43
Zr	284.8 (17.8)	288.7 (2.5)	529.8 (41.6)	531.6 (12.6)	-	182.0 (25.5)	-	2.12	-

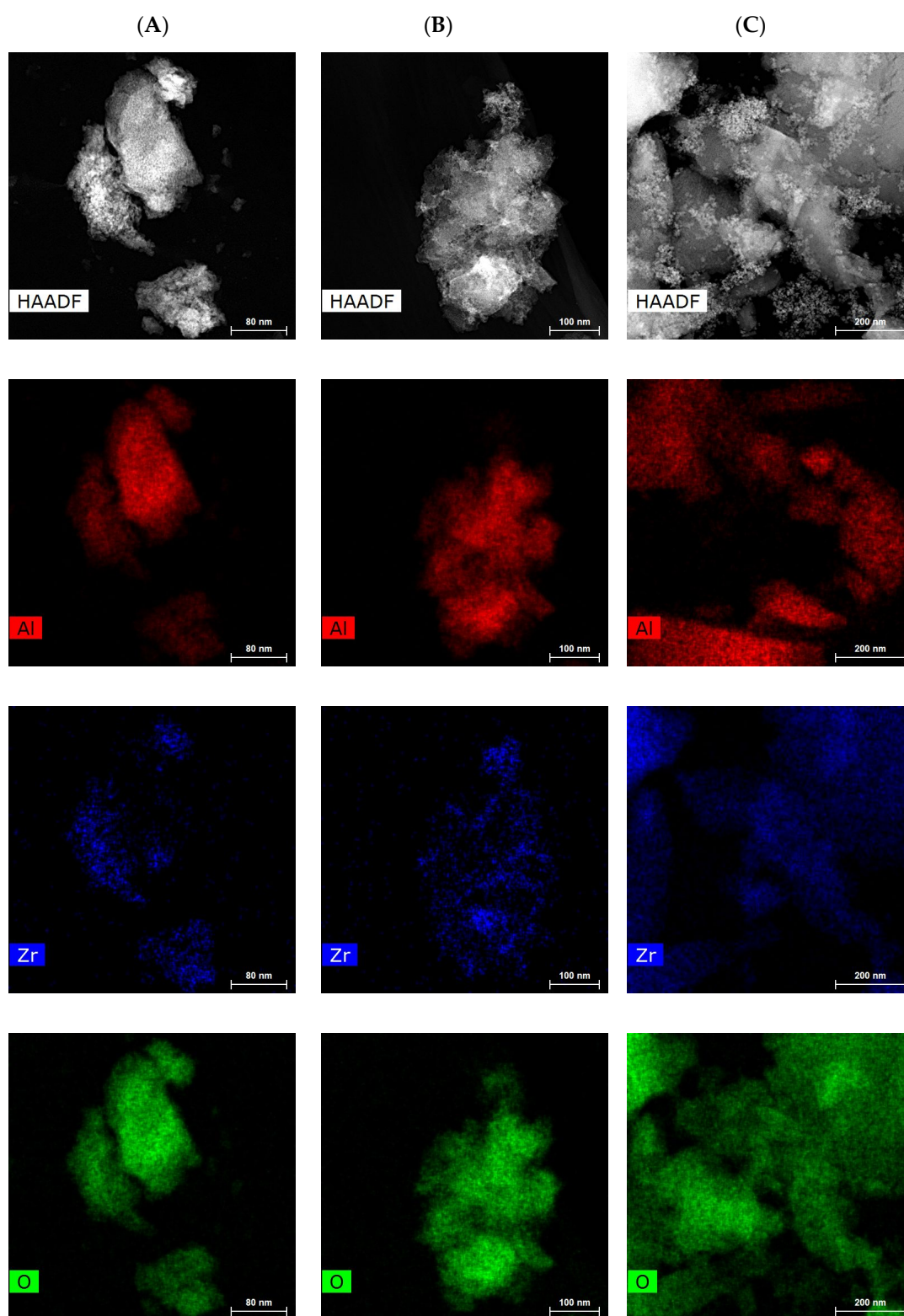


Figure 3. STEM-HAADF (High-angle annular dark-field) images of mixed AlZr oxides. (A) Al_7Zr_3 (B) Al_5Zr_5 , and (C) Al_3Zr_7 .

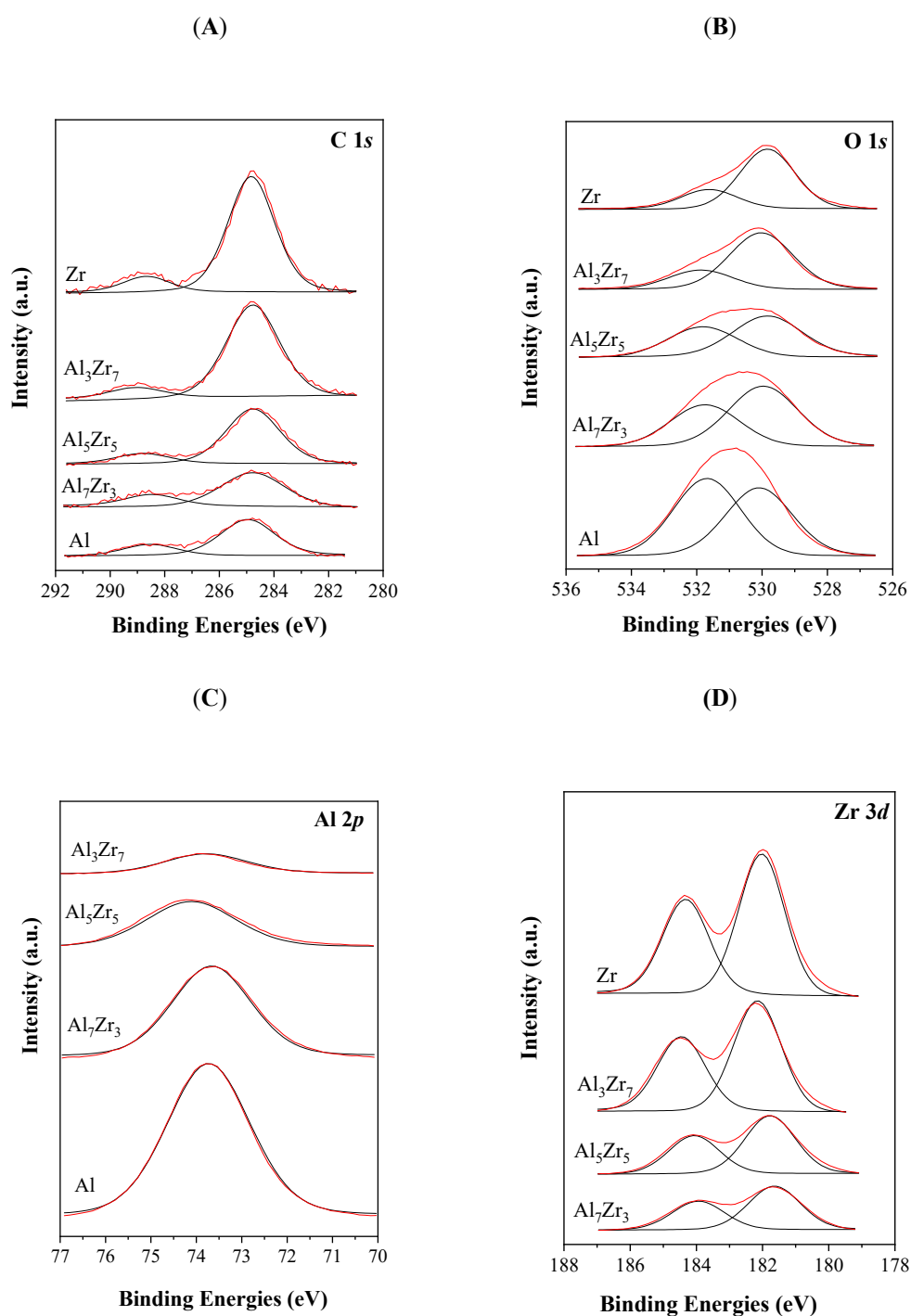


Figure 4. XPS spectra for Al, Zr, and Al_xZr_y catalysts in the (A) C 1s, (B) O 1s, (C) Al 2p, and (D) Zr 3d_{5/2} regions.

On the other hand, the existence of distorted or incomplete coordination spheres, especially on the surface, can affect catalytic activity. Therefore, ²⁷Al NMR was used to determine the aluminum coordination in Al and Al_xZr_y catalysts (Figure 5). Thus, three bands were observed at 9.1, 35.0, and 69.0 ppm, corresponding to octahedral, pentahedral and tetrahedral aluminum species, respectively [63], which were deconvoluted and their pertinent contributions were indicated in Figure 5. The NMR spectrum of Al catalyst showed a more intense peak about 9 ppm, which has been previously observed for boehmite in the literature, being attributed to octahedrally coordinated aluminum sites [55,64]. This fact agrees with results obtained by XRD and XPS. However, a small fraction (2%) of AlO₄

sites was also detected, associated to the disordered nature of boehmite framework sites [64]. It is noteworthy that typical octahedral and tetrahedral chemical shifts move upfield with the increasing amount of zirconium. In the case of Al_3Zr_7 catalyst, octahedral and tetrahedral aluminum peaks were found at 5.3 and 63.7 ppm, respectively, which might be due to the presence of zirconium modified the aluminum environment, or aluminum shielding caused by nearby zirconium atoms. In addition, the peak attributed to tetrahedral aluminum is more intense for mixed metal oxides, especially for Al_5Zr_5 catalyst, reaching a value of 23.3%. It has been previously reported that $\gamma\text{-Al}_2\text{O}_3$ could be formed after thermal treatment at 300 °C, giving rise to an increase in the tetrahedral Al signal [65]. Considering that Al_5Zr_5 catalyst showed both the highest amount of tetrahedral Al species and a higher BE value for Al 2p, as determined by XPS, it would be likely that this catalyst possesses a higher proportion of aluminum oxide phase than the rest of catalysts. This catalyst also showed a small contribution of penta-coordinated Al sites, which had been previously identified in $\gamma\text{-Al}_2\text{O}_3$, but with a relatively low intensity [65,66]. On the other hand, this peak associated to pentahedral, or distorted tetrahedral/octahedral sites, at 30–40 ppm, is only observed after Zr incorporation, being even more intense than the other contributions for Al_3Zr_7 catalyst (45.8%).

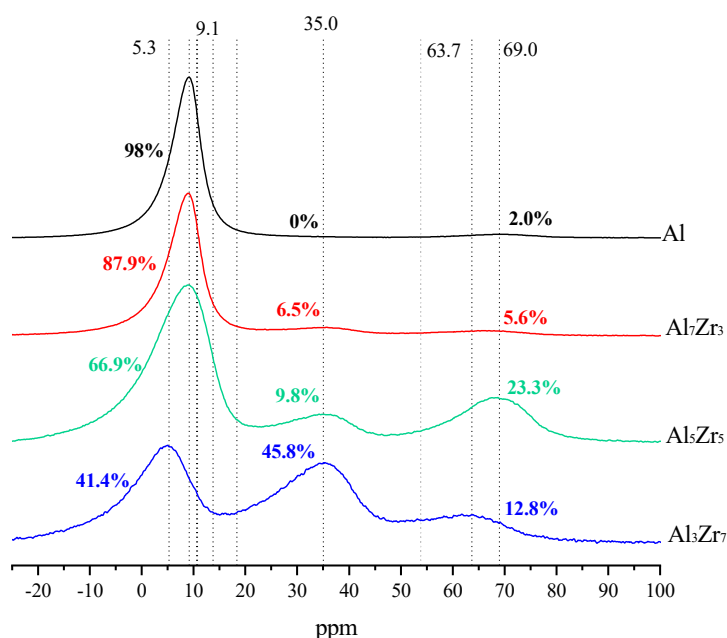


Figure 5. ^{27}Al magic angle spinning-nuclear magnetic resonance (MAS-NMR) of Al and Al_xZr_y catalysts.

Considering the key role of acid sites in the dehydration of glucose into HMF, the acid properties were evaluated by temperature-programmed desorption (TPD) of NH_3 (Table 1). The Al and Al_5Zr_5 catalysts showed the highest total acidity values, although the density of acid sites (expressed per surface unit) was higher for the sample with Zr. However, the rest of catalysts was less acidic, mainly the Zr catalyst. Likewise, the basic properties of catalysts are important, inasmuch basic sites could catalyze the isomerization of glucose to fructose. The data obtained from CO_2 -TPD (Table 1) reveal that these two catalysts (Al and Al_5Zr_5) also exhibited the highest basicity, but their differences with the rest of catalyst were lower than those observed for acid sites. Similarly, the Zr catalyst showed the lowest total basicity, thus becoming the catalyst with the lowest concentration of both acid and basic sites.

2.2. Catalytic Results

Glucose dehydration into HMF is a complex process, which can give rise to different unwanted products, such as levulinic acid, formic acid, and humins [29,67], among others, due to the high

reactivity of HMF. In order to minimize the formation of by-products, an organic co-solvent (MIBK) has been employed to facilitate the extraction of HMF from the aqueous phase [22,25,26,68–70]. This solvent, MIBK, has been classified by the CHEM21 as a recommended solvent, because it does not present severe safety problems, it is not dangerous to health or environmental harmful [71]. Likewise, the addition of inorganic salts has also demonstrated to enhance HMF yield [25,26,70]. In particular, calcium cations have showed an excellent performance [22,72], since their interaction with glucose molecules shifted the anomeric equilibrium toward the glucose α -anomer, in such a way that glucose dehydration took place more readily, improving HMF yield. In a previous work, García Sancho et al. [22] found the optimal amount of calcium chloride was 0.65 g per gram of water, which was also employed in the catalytic tests of the present work to enhance HMF yield.

Firstly, all catalysts were evaluated in the dehydration of glucose at 175 °C (Figure 6), attaining high conversion values. However, the catalysts with higher Al/Zr ratio provided faster glucose conversion rates, which may be due to their higher acidity (Table 1). Thus, full glucose conversion was reached after 60 min with Al, Al₇Zr₃, and Al₅Zr₅ catalysts, whereas a longer reaction time (180 min) is required for Al₃Zr₇ and Zr catalysts (Figure 6A). Moreover, the Al₅Zr₅ catalyst exhibited the highest glucose conversion rate probably due to this material possesses the greatest density of acid sites, which accelerated the transformation of glucose molecules. It should be noted that the presence of the aluminum oxide phase was suggested for this catalyst from XPS and ²⁷Al MAS-NMR analyses, which could explain its higher conversion rate. Regarding HMF yield (Figure 6B), the greatest values were achieved between 30–60 min in all cases, attaining a maximum value of 47% with the Al₃Zr₇ catalyst, after 60 min at 175 °C. Moreover, after reaching the maximum HMF yield, side reactions gained importance, causing the degradation of HMF. This fact can be corroborated by mass balance, which continuously decreased along the reaction, due to side reactions gave rise to by-products, such as soluble and insoluble polymers, which are not detected by HPLC analysis (Figure 6C). This fact was more pronounced for Al₅Zr₅ catalyst, mainly at short reaction times; therefore, aluminum oxide seems to be more active, but secondary reactions are also favored, as previously reported in the literature [22]. This catalyst had also shown slightly higher microporosity that would facilitate the blocking of active sites. It is noteworthy the absence of levulinic and formic acids, which are common HMF rehydration products [11,29]. The least active catalysts, Zr and Al₃Zr₇, showed better carbon balance, mainly at shorter reaction times, probably due to their slower glucose conversion rates. It should be noted that the Al₃Zr₇ catalyst possesses a lower surface Al/Zr molar ratio, as determined by XPS, than nominal value, as well as the highest percentage of pentacoordinated aluminum species (45.8%), as deduced by ²⁷Al MAS-NMR. Although its conversion rate was slower, it was able to provide the highest HMF yield after 60 min at 175 °C. Thus, this catalytic performance could be related to its lower surface Al content, existing more available Zr sites, and/or the higher concentration of pentacoordinated Al species.

It has been shown that the Al₇Zr₃ and Al₅Zr₅ catalysts were the most active catalysts with the fastest conversion rates and HMF yields. However, the possible presence of alumina rather than boehmite for Al₅Zr₅ catalyst could have accelerated the formation of humins, decreasing faster the carbon balance, as previously indicated. Likewise, the Al₃Zr₇ catalyst showed the highest HMF selectivity and, in spite of its lower glucose conversion, the greatest HMF yield (46.5%). Although high conversion values were obtained in all cases, HMF yield did not exceed 50% due to secondary reactions. To decrease these unwanted processes, Al₇Zr₃ and Al₃Zr₇ catalysts were tested at lower reaction temperature, 150 °C, favoring those pathways more kinetically viable at that temperature (Figure 7).

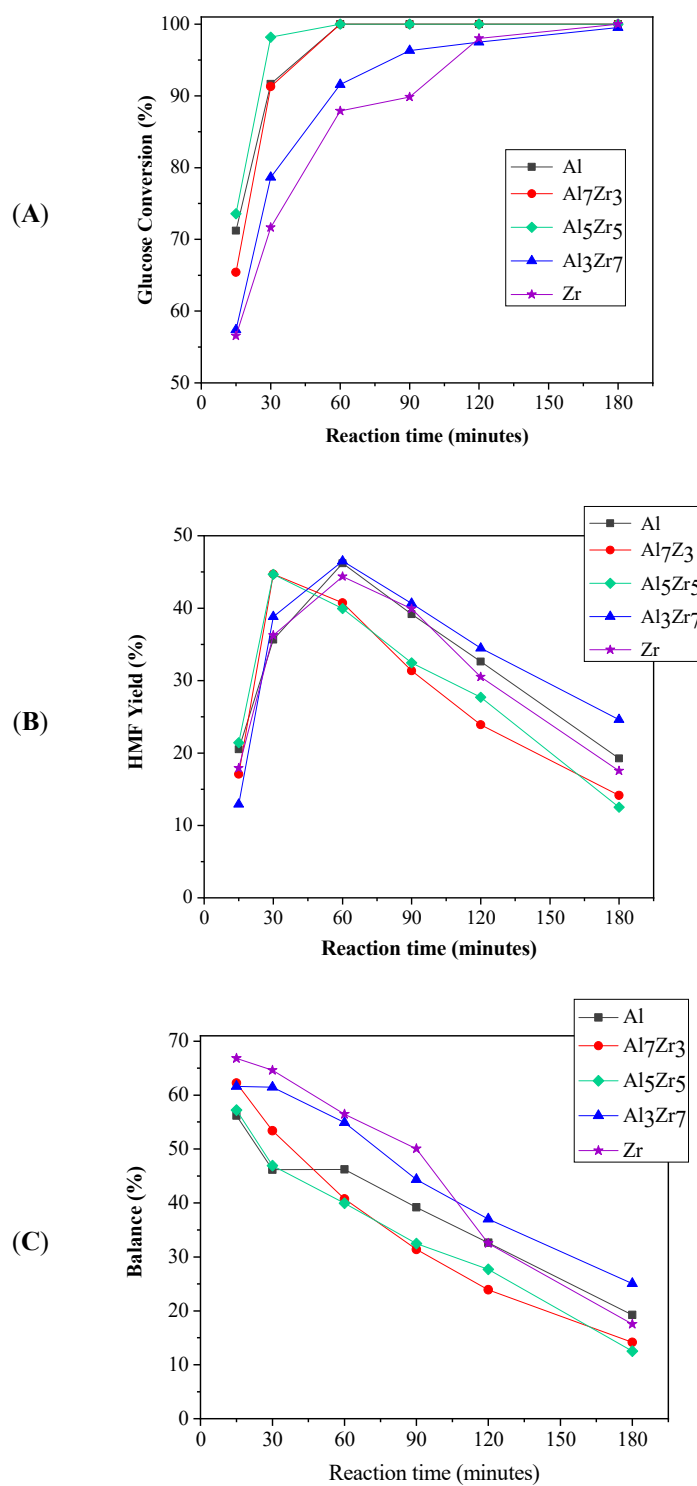


Figure 6. Glucose conversion (A), HMF yield (B), and carbon balance (C) as function of reaction time in the presence of Al, Zr, and Al_xZr_y catalysts (175 °C, 0.65 g CaCl₂·8aq.sol.⁻¹ and glucose/catalyst weight ratio of 3).

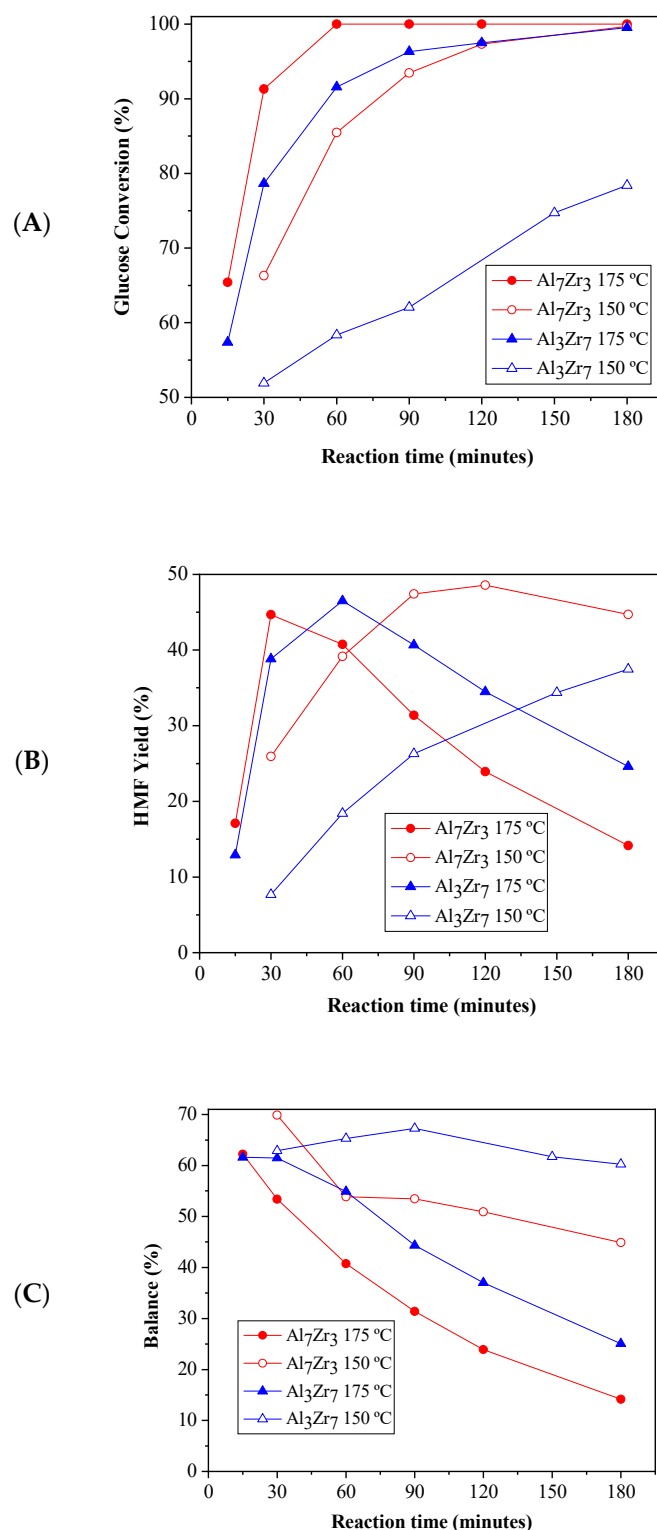


Figure 7. Effect of reaction temperature on glucose conversion (A), HMF yield (B), and carbon balance (C) as a function of reaction time, in the presence of Al₇Zr₃ and Al₃Zr₇ catalysts. Experiments were represented with full and empty symbol for 175 °C and 150 °C, respectively (0.65 g CaCl₂·g_{aq.sol.}⁻¹ and glucose/catalyst weight ratio of 3).

As expected, the catalytic activity was lower at 150 °C for both catalysts and longer reaction times than those observed at 175 °C were required to attain a high glucose conversion (Figure 7A). In the case of Al₇Zr₃, total conversion was achieved after 180 min at 150 °C, whereas Al₃Zr₇ only obtained

a glucose conversion of 78.4% under similar experimental conditions. With regard to HMF yield (Figure 7B), similar values than those obtained at 175 °C were found for longer reaction times. Indeed, the HMF yield was slightly higher (48.6%) in the case of Al_7Zr_3 , after 120 min at 150 °C, than the maximum value obtained at 175 °C (44.6%) in spite of the glucose conversion at 150 °C was lower. This maximum HMF yield obtained after 120 min in the presence of Al_7Zr_3 started to decrease from 180 min, although the HMF degradation occurred much slower than at higher reaction temperature. This fact corroborates that secondary reactions are unfavored at lower reaction temperature. In the case of Al_3Zr_7 , the maximum HMF yield obtained at 150 °C (37.5%) was lower than that achieved at 175 °C, needing longer reaction times to attain the maximum HMF yield, since its value was still growing after 180 min at 150 °C (Figure 7B). Therefore, the Al_7Zr_3 catalyst, with mostly octahedral aluminum species, would be more active than Al_3Zr_7 , which displayed a high proportion of penta- and tetra-coordinated aluminum species. On the other hand, the mass balances (Figure 7C) were better than those obtained at 175 °C, mainly for the least active Al_3Zr_7 , even at longer reaction times. This fact would demonstrate again that the side reactions were unfavored at 150 °C.

The positive effect of adding CaCl_2 on the catalytic performance was also corroborated (Figure 8), since both glucose conversion and HMF yield significantly increased. Thus, the interaction of calcium cations with glucose molecules shifts the anomeric equilibrium towards the α -anomer, more prone to be dehydrated to HMF, as previously demonstrated [22]. The presence of CaCl_2 promoted both glucose isomerization and fructose dehydration, since the concentration of fructose was higher when reaction was carried out in the absence of calcium chloride. Consequently, HMF yield decreased under 10%, demonstrating that the presence of CaCl_2 considerably enhances the HMF production. Indeed, García-Sancho et al. indicated that Ca^{2+} could also interact with fructose molecules [22]. In any case, the combined use of CaCl_2 and Al_7Zr_3 provided better catalytic results than if salt, or catalyst, was only utilized.

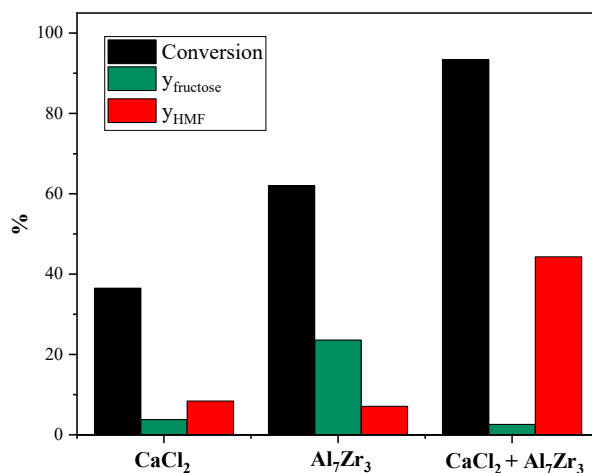


Figure 8. Effect of adding CaCl_2 without or with Al_7Zr_3 catalyst (150 °C, 90 min, glucose/catalyst weight ratio of 3 and/or $0.65 \text{ g CaCl}_2 \cdot \text{g}_{\text{aq.sol.}}^{-1}$).

The influence of glucose:catalyst weight ratio was also evaluated by modifying both the amount of glucose and catalyst. In the former case, the catalyst loading was constant (0.05 g) and the glucose amount was modified between 0.05 and 0.30 g (Figure 9A). In the latter case, glucose loading was maintained constant (0.15 g) and the amount of catalyst was varied between 0.025 and 0.150 g (Figure 9B). The highest glucose conversion and HMF yield were found for a glucose:catalyst weight ratio of 3:1, when the glucose concentration was modified (Figure 9A). However, the amount of Al_7Zr_3 catalyst was not enough to carry out the glucose transformation into HMF for higher glucose:catalyst weight ratio (6:1). On the other hand, the glucose conversion was barely affected when the glucose concentration was decreased to obtain a glucose:catalyst weight ratio of 1:1, but the HMF yield was

lowered. This fact was probably due to secondary reactions, subsequently decreasing the HMF yield. Likewise, the highest HMF yield was found for a glucose:catalyst weight ratio of 3:1 when the quantity of catalyst was varied (Figure 9B). However, differences with other ratios (6:1 and 1:1) were negligible, which would indicate that secondary reactions are more favorable in excess of glucose, and consequently of HMF produced, than in the presence of a higher amount of catalyst.

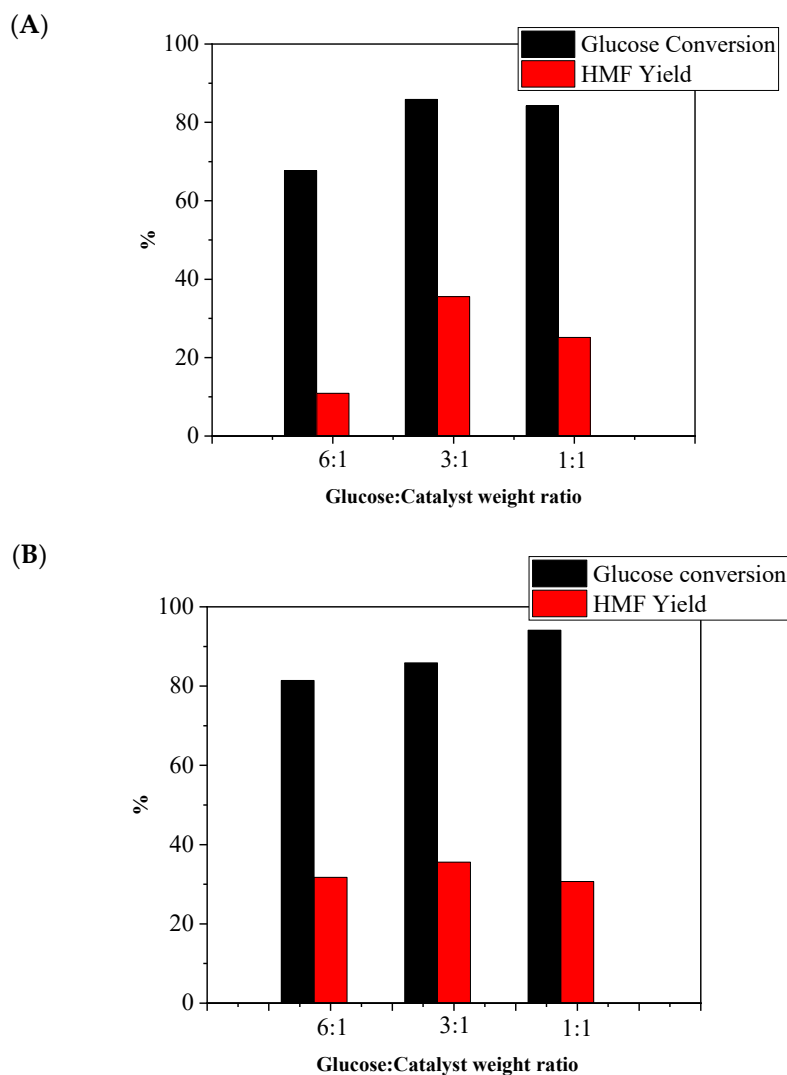


Figure 9. Influence of glucose: Al_7Zr_3 weight ratio, by modifying the amount of glucose (A) or catalyst (B), on the catalytic performance ($150\text{ }^\circ\text{C}$, 60 min and $0.65\text{ g CaCl}_2\cdot\text{g}_{\text{aq.sol.}}^{-1}$).

Considering these catalytic data, a glucose:catalyst weight ratio of 3:1 was employed to study the reuse of Al_7Zr_3 to facilitate its handling between cycles. In the recyclability study, each catalytic run was carried out for 60 min at $150\text{ }^\circ\text{C}$, in the presence of Al_7Zr_3 and CaCl_2 (Figure 10). After each run, both water and MIBK were extracted, whereas the catalyst was maintained at the bottom of the reactor, subsequently dried at $70\text{ }^\circ\text{C}$, and employed in the next catalytic run without any pretreatment. The Al_7Zr_3 catalyst roughly maintained its activity for four cycles, in spite of glucose conversion slightly decreased, with HMF yields between 28% and 37%. However, both conversion and HMF yield got worse from the fifth cycle, which could be due to losses of catalyst by manipulation between cycles, or its deactivation as a consequence of the formation of organic deposits, which would block acid sites. After recovering the Al_7Zr_3 catalyst after the sixth cycle, it was observed that the solid had become deliquescent, which complicated severely its characterization. It must be taken into account that

different products from polymerized glucose, fructose, furan compounds, or other organic substances, including MIBK, water, and calcium chloride, could be partially covering the used catalyst.

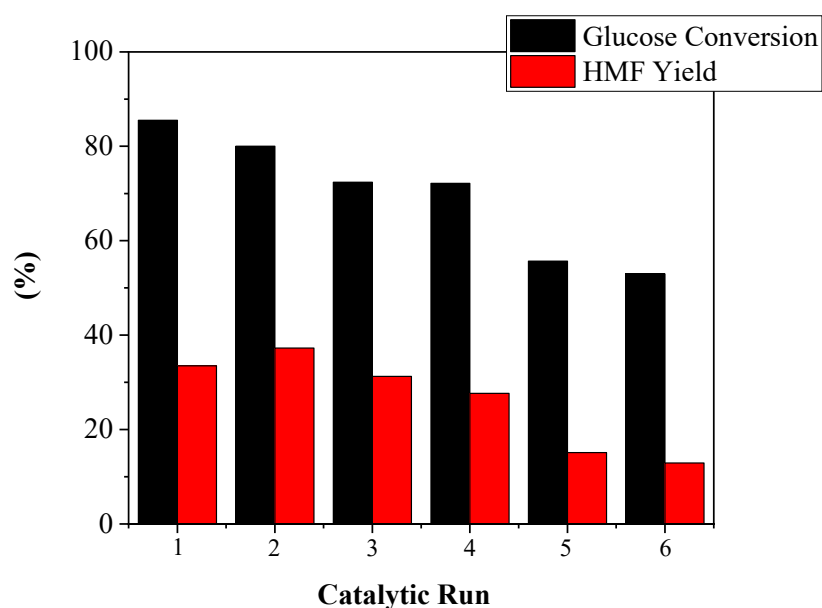


Figure 10. Reutilization study for Al_7Zr_3 catalyst (150 °C, 60 min, glucose/catalyst weight ratio of 3 and $0.65 \text{ g CaCl}_2 \cdot 8\text{aq.sol.}^{-1}$).

Nevertheless, it was analyzed by Differential Thermal Analysis and Thermogravimetry (DTA–TG) up to 300 °C, which was the calcination temperature of catalysts, since higher temperatures could lead to phase transformations of mixed metal oxides, rendering even more difficult the interpretation of thermogravimetric data (Figure 11). The TG curve exhibits a continuous weight loss of 27.5%, extending from room temperature until 300 °C, which is associated to a broad and intense endothermic peak centered at 62 °C and another smaller one at 134 °C. Furthermore, heat flow indicated that the low temperature effect corresponds to an evaporation enthalpy of $2330 \text{ J} \cdot \text{g}^{-1}$, which is typical of water. Moreover, it is well known that calcium chloride is deliquescent, and water could be associated to this salt. On the other hand, the second peak presented a vaporization heat of $553 \text{ J} \cdot \text{g}^{-1}$ which is intermediate between vaporization enthalpy values of MIBK and HMF (366 and $718 \text{ J} \cdot \text{g}^{-1}$, respectively), having the former a boiling point of 116 °C. Thereby, weight losses could be explained by the dehydration of deliquescent CaCl_2 , and the vaporization of MIBK and HMF adsorbed on the catalyst surface.

Therefore, it has been demonstrated that mixed AlZr oxides displayed a higher catalytic activity, in the dehydration of glucose to HMF, than the corresponding pure metal oxides, and even other mixed metal oxides reported in the literature. Thus, a 47% HMF yield was attained at 150 °C after 2 h, or after shorter reaction time (1 h), but at higher temperature (175 °C). Zhang et al. [46] studied the catalytic performance in glucose dehydration of zirconia calcined at different temperatures, finding that the most acidic zirconia (an amorphous phase), obtained after calcination at 300 °C, only achieved an HMF yield of 35% in a dimethyl sulfoxide–water biphasic system at 170 °C, but 4 h of reaction were required. Likewise, Stošić et al. [73] synthesized crystalline zirconium oxide supported over mesostructured amorphous niobium oxide, aiming to benefit from interactions between and the support to generate active sites for the dehydration. In this case, only an HMF yield of 26% was achieved after 6 h from 1 wt.% fructose solutions at 130 °C, but using more concentrated solutions, and the catalyst was deactivated due to carbonaceous deposits covering active sites. In contrast, Atanda et al. [48] tested glucose dehydration by using zirconium-titanium oxides catalysts in water at 160 °C for 5 h. They obtained a 23.6% yield for Ti:Zr 1:1 catalyst, which enhanced up to 71% in the presence of THF (tetrahydrofuran), as co-solvent, and NaCl, but an additional Brønsted co-catalyst, Amberlyst–70, was employed. On the other hand, Córdova-Pérez et al. [74] prepared a series of

Al-Ti-W oxides, achieving approximately a 70% HMF yield in a biphasic system H₂O:THF in the presence of NaCl, at 175 °C for 3 h, under 3 MPa of Argon. Thus, these mixed Al and Zr oxides were able to provide relevant values of HMF yields under less drastic conditions than others previously reported in the literature.

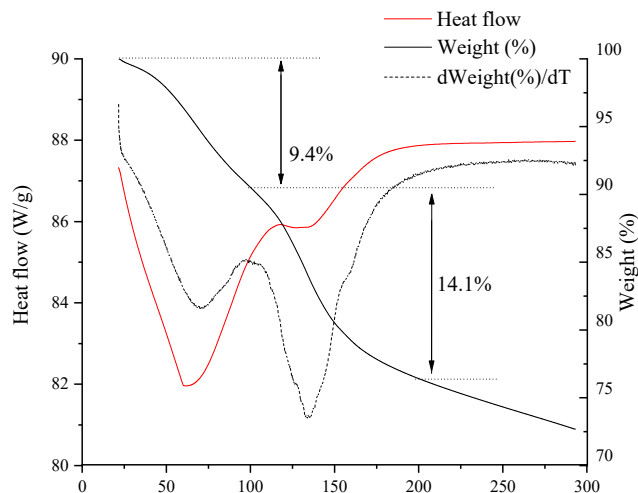


Figure 11. Differential Thermal Analysis and Thermogravimetry (DTA–TG) analysis of Al₇Zr₃ catalyst recovered after 6th catalytic run of reuse.

Finally, Al₇Zr₃ and Al₃Zr₇ have been tested for HMF production from cellulose at 175 °C for 2 h by using a cellulose:catalyst weight ratio of 3:1 and CaCl₂ to check if these materials were able to carry out both hydrolysis and dehydration reactions. Under these experimental conditions, HMF was detected with HMF yield values (expressed as mass of obtained HMF/mass of cellulose × 100) equal to 3.5 and 4.5 wt.% for Al₇Zr₃ and Al₃Zr₇, respectively. Although these values were low and reaction conditions should be optimized by using cellulose as feedstock, they demonstrated that these catalysts were able to catalyze both hydrolysis of cellulose and dehydration of pertinent monomers into HMF. However, degradation of cellulose requires temperatures above 200 °C, as it has been pointed out in the literature [75].

3. Materials and Methods

3.1. Reagents

Aluminum nitrate nonahydrate 99% (Sigma-Aldrich, St. Louis, MO, USA), zirconyl chloride octahydrate 98% (Sigma-Aldrich, St. Louis, MO, USA), D-(+)-Glucose 99% (Sigma-Aldrich, St. Louis, MO, USA), calcium chloride (Sigma-Aldrich, St. Louis, MO, USA), methyl isobutyl ketone 100% (VWR Chemicals, Radnor, PA, USA), methanol 99.9% (Panreac, Castellar del Vallès, Spain), ammonia 28% (VWR Chemicals, Radnor, PA, USA), and deionized water were used.

3.2. Catalyst Synthesis

A series of mixed Al-Zr oxides with different Al:Zr molar ratio (10:0, 7:3, 5:5, 3:7, and 0:10) was prepared by coprecipitation, following the method proposed by He et al. [76]. First, the corresponding quantities of aluminum and zirconium precursors (total metal amount of 30 mmol) were dissolved in 200 mL of deionized water under constant stirring. The precipitation of metal hydroxides was achieved by slow addition of ammonia until pH = 9. The resulting gel was stirred for other 5 h for complete homogenization. The precipitate was collected by filtration and thoroughly washed with deionized water until neutral pH. All samples were dried at 80 °C for 16 h, then calcined at 300 °C for 4 h with a heating rate of 5 °C·min⁻¹. The catalysts based on pure aluminum and zirconium oxides

were denominated as Al and Zr, respectively, and mixed metal oxides were denoted as Al_xZr_y , where x and y indicated mol of aluminum and zirconium, respectively.

3.3. Characterization of Catalysts

Powder diffraction patterns were obtained on a Philips EMPYREAN automated diffractometer using $Cu\ K\alpha_{1,2}$ (1,5406 Å) and a PIXcel detector (Royston, UK). Divergence and antivergence slits were fixed at $1/2^\circ$. Soller slits for incident and refracted rays were employed at 0.04 rads. Measures were taken from 5 to 80° (2θ) for approximately 30 min with a step size of 0.0167° . The X-ray tube voltage employed was 45 kV and current of 40 mA. The sample was rotated continuously to increase particle statistics.

Magic angle spinning-nuclear magnetic resonance (MAS-NMR) spectra of ^{27}Al were recorded with an AVANCEIII HD 600 (Bruker AXS, Rheinstetten, Germany) using Hpdect technique. Samples were rotated with a speed of 20 kHz in 2.5 mm triple resonance DVT probes. 5000 scans were carried out for each sample with 1 s delay. Chemical shifts were referenced to $Al(NO_3)_3$. For the analysis, a magnetic field of 14.1 T corresponding to a ^{27}Al resonance frequency of 156.37 MHz was used.

Transmission electron microscopy (TEM) images were acquired by using a FEI Talos F200X (Thermo Fisher Scientific, Waltham, MA, USA) equipped with a CMOS camera of 16 megapixels. Chemical homogeneity in catalyst particles was analyzed by EDX mapping, taken in STEM-HAADF mode.

X-ray photoelectron spectra (XPS) were collected using a Physical Electronics PHI5700 (Eden Prairie, Minnesota, USA). Measurements were carried out with monochromatic $Mg\ K\alpha$ radiation (300 W and 1253.6 eV) and multichannel detector in FAT mode (29.35 eV). Analysis area was set to 720 μm . All binding energies were calibrated respect to C 1s peak of adventitious carbon at 284.8 eV. Physical Electronics Multipack 9.6 software was employed to process all XPS data (Version 9.6, Physical Electronics Inc., Chanhassen, MN, USA, 2003).

N_2 adsorption-desorption isotherms at $-196^\circ C$ were determined with an automatic gas adsorption ASAP 2420 surface area and porosity analyzer model (Micromeritics, Norcross, GA, U.S.A). Samples were previously evacuated at $200^\circ C$ and 10^{-4} mbar for 24 h. Specific surface areas were calculated by taking a nitrogen molecule cross section of $16.2\ \text{\AA}^2$ and using the Brunauer-Emmet-Teller (BET) equation. Pore size distributions were obtained using the DFT (Density Functional Theory) method.

Temperature-programmed desorption of ammonia (NH_3 -TPD) and carbon dioxide (CO_2 -TPD) were recorded in order to evaluate the surface acidity and basicity of the catalysts, respectively. In the case of NH_3 -TPD, 0.08 g of each sample were evacuated under helium flow by heating up to the calcination temperature ($300^\circ C$), and then, after cooling, the adsorption of ammonia was performed at $100^\circ C$. The NH_3 -TPD was carried out by increasing the temperature from 100 to $300^\circ C$, with a heating rate of $5^\circ C\cdot min^{-1}$, maintaining at this temperature for 15 min and using a helium flow of $40\ mL\ min^{-1}$. CO_2 adsorption was similarly carried out by using 0.2 g of catalyst and performing CO_2 adsorption at $80^\circ C$. The evolved gases (ammonia and carbon dioxide) were analyzed using a thermal conductivity detector (TCD) (Shimadzu, Kyoto, Japan).

3.4. Catalytic Tests

The reactions were carried out under batch conditions, by using glass pressure tubes with thread bushing (Ace, 15 mL) in a temperature-controlled aluminum block under magnetic stirring. Experiments usually consisted on 1.5 mL of deionized water, 3.5 mL MIBK, 0.05 g of catalyst, 0.15 g of glucose, and 0.65 g $CaCl_2$ per g H_2O . Reactors were purged with N_2 before reaction to avoid unwanted reactions. Once the reactions finished, the reactors were removed from the aluminum block and submerged in cool water to stop the catalytic process. Analysis of both phases was performed through high performance liquid chromatography (HPLC). A JASCO instrument equipped with quaternary gradient pump (PU-2089), multiwavelength detector (MD-2015), autosampler (AS-2055), and column oven (co-2065) was employed. Aqueous and organic phases were analyzed by employing different columns, Phenomenex Rezex ROA-Organic Acid H^+ (8%) ($300\ mm \times 7.8\ mm$ and $5\ \mu m$)

and Phenomenex Luna C18 reversed-phase column (250 mm × 4.6 mm and 5 μm) respectively, by using 0.005 N H₂SO₄ solution (flow rate 0.35 mL min⁻¹) and pure methanol (flow rate 0.5 mL min⁻¹) as mobile phases at 40 °C and room temperature respectively. Glucose and fructose were quantified using a refractive index detector for aqueous phase, whereas HMF was quantified by a UV detector in both phases. Glucose conversion, HMF selectivity, HMF yield and carbon balance were calculated as follows:

$$\begin{aligned} \text{Conversion}_{\text{Glucose}} &= \frac{\text{Glucose}_{\text{initial}} - \text{Glucose}_{\text{final}}}{\text{Glucose}_{\text{initial}}} \cdot 100 \\ \text{Selectivity}_{\text{HMF}} &= \frac{\text{HMF}_{\text{final}}}{\text{Glucose}_{\text{initial}} - \text{Glucose}_{\text{final}}} \cdot 100 \\ \text{Yield}_{\text{HMF}} &= \frac{\text{Selectivity}_{\text{HMF}} \cdot \text{Conversion}}{100} \\ \text{Balance} &= \frac{\text{HMF}_{\text{final}} + \text{Glucose}_{\text{final}} + \text{Fructose}_{\text{final}}}{\text{Glucose}_{\text{initial}}} \cdot 100 \end{aligned}$$

4. Conclusions

A series of Al_xZr_y oxide catalysts was synthesized by coprecipitation of metal hydroxides and subsequent calcination. A boehmite phase was identified by XRD and XPS analyses for the Al catalyst, not being possible to distinguish between oxides and oxohydroxides for mixed metal oxides. In particular, the Al₅Zr₅ catalyst could present pseudoboehmite or alumina phases, which were not detected for the rest of catalysts. In addition, amorphous zirconia prevented structural identification of Zr phases. Total acidity and basicity, as well as site densities, decreased progressively with the zirconium content, in such a way that higher Al content provided more acidic and basic catalysts, according to its amphoteric character. The Al₅Zr₅ catalyst did not follow this trend due to its different superficial nature, showing acid–base properties similar to those of pure Al catalyst. As expected, catalysts with the highest concentration of active sites achieved total conversion faster, although this superior activity was also responsible for lower carbon balance values caused by promotion of secondary reactions. The Al₃Zr₇ catalyst, being less active and needing longer reaction time, gave rise to the best selectivity (50%) and yield (46%) at 175 °C. Therefore, it was also observed that the presence of octahedral Al sites accelerated glucose dehydration into HMF, causing sooner their deactivation for high Al content catalysts. However, a lower catalytic activity was found for Zr-rich catalysts, but deactivation was also slower in such a way that the presence of pentacoordinated Al and/or a lower Al content for Al₃Zr₇ catalyst led to the highest HMF yield. On the other hand, the reduction of reaction temperature, as expected, led to longer reaction times to attain similar HMF yields, but side reactions were partially avoided, yielding better carbon balance values. Moreover, both HMF yield and selectivity obtained at 150 °C were similar to those obtained at 175 °C, suggesting glucose dehydration route was similarly affected than secondary reaction paths and activation energies should be close. Likewise, Al_xZr_y catalysts could be reused at least for four catalytic runs, but their catalytic activity started to decrease from the fifth cycle probably due to the deposition of organic molecules.

Author Contributions: Experiment: B.T.-O. and S.M.-M.; Data Curation: B.T.-O., C.G.-S., and J.A.C.; Writing-Original Draft Preparation: B.T.-O., C.G.-S., and P.M.-T.; Writing-Review & Editing: C.G.-S., J.A.C., and P.M.-T.; Supervision: C.G.-S. and P.M.-T.; Funding Acquisition: C.G.-S. and P.M.-T. All authors have read and agreed to the published version of the manuscript.

Funding: This research was funded by the Spanish Ministry of Economy and Competitiveness (RTI2018-94918-B-C44), FEDER (European Union) funds (UMA18-FEDERJA-171) and Malaga University.

Acknowledgments: B.T.-O. and J.A.C. thank to the Malaga University for the financial support. C.G.-S. acknowledges FEDER funds for a postdoctoral contract (UMA18-FEDERJA-171).

Conflicts of Interest: The authors declare no conflict of interest.

References

1. Breitburg, D.; Levin, L.A.; Oschlies, A.; Grégoire, M.; Chavez, F.P.; Conley, D.J.; Garçon, V.; Gilbert, D.; Gutiérrez, D.; Isensee, K.; et al. Declining Oxygen in the Global Ocean and Coastal Waters. *Science* **2018**, *359*, eaam7240. [[CrossRef](#)]
2. United Nations Environment Programme. *Emissions Gap Report 2019*; UNEP: Nairobi, Kenya, 2019.
3. IPCC. *Global Warming of 1.5 °C*; Masson-Delmotte, V., Zhai, P., Pörtner, H.O., Roberts, D., Skea, J., Pirani, P.R.S.A., Moufouma-Okia, W., Péan, C., Pidcock, R., Connors, S., Eds.; IPCC: Geneva, Switzerland, 2018.
4. Werpy, T.; Petersen, G. *Top Value Added Chemicals from Biomass: Volume I—Results of Screening for Potential Candidates from Sugars and Synthesis Gas*; National Renewable Energy Lab.: Golden, CO, USA, 2004.
5. Klemm, D.; Heublein, B.; Fink, H.P.; Bohn, A. Cellulose: Fascinating Biopolymer and Sustainable Raw Material. *Angew. Chem. Int. Ed.* **2005**, *44*, 3358–3393. [[CrossRef](#)] [[PubMed](#)]
6. Yousuf, A.; Pirozzi, D.; Sannino, F. Fundamentals of Lignocellulosic Biomass. In *Lignocellulosic Biomass to Liquid Biofuels*; Academic Press: Cambridge, MA, USA, 2020; pp. 1–15.
7. McGlone, J.; Priece, P.; da Vià, L.; Majdal, L.; Lopez-Sanchez, J. Desilicated ZSM-5 Zeolites for the Production of Renewable p-Xylene via Diels–Alder Cycloaddition of Dimethylfuran and Ethylene. *Catalysts* **2018**, *8*, 253. [[CrossRef](#)]
8. Hu, L.; Tang, X.; Xu, J.; Wu, Z.; Lin, L.; Liu, S. Selective Transformation of 5-Hydroxymethylfurfural into the Liquid Fuel 2,5-Dimethylfuran over Carbon-Supported Ruthenium. *Ind. Eng. Chem. Res.* **2014**, *53*, 3056–3064. [[CrossRef](#)]
9. Bohre, A.; Dutta, S.; Saha, B.; Abu-Omar, M.M. Upgrading Furfurals to Drop-in Biofuels: An Overview. *ACS Sustain. Chem. Eng.* **2015**, *3*, 1263–1277. [[CrossRef](#)]
10. Alonso, D.M.; Bond, J.Q.; Dumesic, J.A. Catalytic Conversion of Biomass to Biofuels. *Green Chem.* **2010**, *12*, 1493–1513. [[CrossRef](#)]
11. Zhang, J.; Weitz, E. An in Situ NMR Study of the Mechanism for the Catalytic Conversion of Fructose to 5-Hydroxymethylfurfural and Then to Levulinic Acid Using ¹³C Labeled d-Fructose. *ACS Catal.* **2012**, *2*, 1211–1218. [[CrossRef](#)]
12. Shimizu, K.-I.; Uozumi, R.; Satsuma, A. Enhanced Production of Hydroxymethylfurfural from Fructose with Solid Acid Catalysts by Simple Water Removal Methods. *Catal. Commun.* **2009**, *10*, 1849–1853. [[CrossRef](#)]
13. Román-Leshkov, Y.; Moliner, M.; Labinger, J.A.; Davis, M.E. Mechanism of Glucose Isomerization Using a Solid Lewis Acid Catalyst in Water. *Angew. Chem. Int. Ed.* **2010**, *49*, 8954–8957. [[CrossRef](#)]
14. Román-Leshkov, Y.; Barrett, C.J.; Liu, Z.Y.; Dumesic, J.A. Production of Dimethylfuran for Liquid Fuels from Biomass-Derived Carbohydrates. *Nature* **2007**, *447*, 982–985. [[CrossRef](#)]
15. Zhang, J.; Liang, Q.; Xie, W.; Peng, L.; He, L.; He, Z.; Chowdhury, S.P.; Christensen, R.; Ni, Y. An Eco-Friendly Method to Get a Bio-Based Dicarboxylic Acid Monomer 2,5-Furandicarboxylic Acid and Its Application in the Synthesis of Poly(Hexylene 2,5-Furandicarboxylate) (PHF). *Polymers* **2019**, *11*, 197. [[CrossRef](#)] [[PubMed](#)]
16. Kabyemela, B.M.; Adschiri, T.; Malaluan, R.M.; Arai, K. Glucose and Fructose Decomposition in Subcritical and Supercritical Water: Detailed Reaction Pathway, Mechanisms, and Kinetics. *Ind. Eng. Chem. Res.* **1999**, *38*, 2888–2895. [[CrossRef](#)]
17. Tsilomelekis, G.; Orella, M.J.; Lin, Z.; Cheng, Z.; Zheng, W.; Nikolakis, V.; Vlachos, D.G. Molecular Structure, Morphology and Growth Mechanisms and Rates of 5-Hydroxymethyl Furfural (HMF) Derived Humins. *Green Chem.* **2016**, *18*, 1983–1993. [[CrossRef](#)]
18. Román-Leshkov, Y.; Chheda, J.N.; Dumesic, J.A. Phase Modifiers Promote Efficient Production of Hydroxymethylfurfural from Fructose. *Science* **2006**, *312*, 1933–1937. [[CrossRef](#)]
19. Yang, F.; Liu, Q.; Yue, M.; Bai, X.; Du, Y. Tantalum Compounds as Heterogeneous Catalysts for Saccharide Dehydration to 5-Hydroxymethylfurfural. *Chem. Commun.* **2011**, *47*, 4469–4471. [[CrossRef](#)]
20. Rao, K.T.V.; Souzanchi, S.; Yuan, Z.; Ray, M.B.; Xu, C. Simple and Green Route for Preparation of Tin Phosphate Catalysts by Solid-State Grinding for Dehydration of Glucose to 5-Hydroxymethylfurfural (HMF). *RSC Adv.* **2017**, *7*, 48501–48511. [[CrossRef](#)]
21. He, J.; Liu, M.; Huang, K.; Walker, T.W.; Maravelias, C.T.; Dumesic, J.A.; Huber, G.W. Production of Levoglucosenone and 5-Hydroxymethylfurfural from Cellulose in Polar Aprotic Solvent-Water Mixtures. *Green Chem.* **2017**, *19*, 3642–3653. [[CrossRef](#)]

22. García-Sancho, C.; Fúnez-Núñez, I.; Moreno-Tost, R.; Santamaría-González, J.; Pérez-Inestrosa, E.; Fierro, J.L.G.; Maireles-Torres, P. Beneficial Effects of Calcium Chloride on Glucose Dehydration to 5-Hydroxymethylfurfural in the Presence of Alumina as Catalyst. *Appl. Catal. Environ.* **2017**, *206*, 617–625. [[CrossRef](#)]
23. Shimanouchi, T.; Yoshitaka, K.; Tatsuya, T.; Yukioka, K. Chemical Conversion and Liquid–Liquid Extraction of 5-Hydroxymethylfurfural from Fructose by Slug Flow Microreactor. *AIChE J.* **2016**, *62*, 2135–2143. [[CrossRef](#)]
24. Kruger, J.S.; Choudhary, V.; Nikolakis, V.; Vlachos, D.G. Elucidating the Roles of Zeolite H-BEA in Aqueous-Phase Fructose Dehydration and HMF Rehydration. *ACS Catal.* **2013**, *3*, 1279–1291. [[CrossRef](#)]
25. Jiménez-Morales, I.; Moreno-Recio, M.; Santamaría-González, J.; Maireles-Torres, P.; Jiménez-López, A. Production of 5-Hydroxymethylfurfural from Glucose Using Aluminium Doped MCM-41 Silica as Acid Catalyst. *Appl. Catal. Environ.* **2015**, *164*, 70–76. [[CrossRef](#)]
26. Román-Leshkov, Y.; Dumesic, J.A. Solvent Effects on Fructose Dehydration to 5-Hydroxymethylfurfural in Biphasic Systems Saturated with Inorganic Salts. *Top. Catal.* **2009**, *52*, 297–303. [[CrossRef](#)]
27. Pallagi, A.; Dudás, C.; Csédes, Z.; Forgó, P.; Pálkó, I.; Sipos, P. Structure and Equilibria of Ca²⁺-Complexes of Glucose and Sorbitol from Multinuclear (¹H, ¹³C and ⁴³Ca) NMR Measurements Supplemented with Molecular Modelling Calculations. *J. Mol. Struct.* **2011**, *993*, 336–340. [[CrossRef](#)]
28. Blanshard, J.M.V.; Mitchell, J.R. *Polysaccharides in Food*; Elsevier: Amsterdam, The Netherlands, 2013; Volume 2.
29. Van Putten, R.-J.; van der Waal, J.C.; de Jong, E.; Rasrendra, C.B.; Heeres, H.J.; de Vries, J.G. Hydroxymethylfurfural, A Versatile Platform Chemical Made from Renewable Resources. *Chem. Rev.* **2013**, *113*, 1499–1597. [[CrossRef](#)]
30. Choudhary, V.; Mushrif, S.H.; Ho, C.; Anderko, A.; Nikolakis, V.; Marinkovic, N.S.; Frenkel, A.I.; Sandler, S.I.; Vlachos, D.G. Insights into the Interplay of Lewis and Brønsted Acid Catalysts in Glucose and Fructose Conversion to 5-(Hydroxymethyl)Furfural and Levulinic Acid in Aqueous Media. *J. Am. Chem. Soc.* **2013**, *135*, 3997–4006. [[CrossRef](#)] [[PubMed](#)]
31. Saravanamurugan, S.; Paniagua, M.; Melero, J.A.; Riisager, A. Efficient Isomerization of Glucose to Fructose over Zeolites in Consecutive Reactions in Alcohol and Aqueous Media. *J. Am. Chem. Soc.* **2013**, *135*, 5246–5249. [[CrossRef](#)]
32. Jiménez-Morales, I.; Teckchandani-Ortiz, A.; Santamaría-González, J.; Maireles-Torres, P.; Jiménez-López, A. Selective Dehydration of Glucose to 5-Hydroxymethylfurfural on Acidic Mesoporous Tantalum Phosphate. *Appl. Catal. Environ.* **2014**, *144*, 22–28. [[CrossRef](#)]
33. Moreau, C.; Durand, R.; Roux, A.; Tichit, D. Isomerization of Glucose into Fructose in the Presence of Cation-Exchanged Zeolites and Hydrotalcites. *Appl. Catal. Gen.* **2000**, *193*, 257–264. [[CrossRef](#)]
34. Delidovich, I.; Palkovits, R. Catalytic Activity and Stability of Hydrophobic Mg-Al Hydrotalcites in the Continuous Aqueous-Phase Isomerization of Glucose into Fructose. *Catal. Sci. Tech.* **2014**, *4*, 4322–4329. [[CrossRef](#)]
35. Delidovich, I.; Palkovits, R. Structure-Performance Correlations of Mg-Al Hydrotalcite Catalysts for the Isomerization of Glucose into Fructose. *J. Catal.* **2015**, *327*, 1–9. [[CrossRef](#)]
36. Liu, C.; Carraher, J.M.; Swedberg, J.L.; Herndon, C.R.; Fleitman, C.N.; Tessonnier, J.P. Selective Base-Catalyzed Isomerization of Glucose to Fructose. *ACS Catal.* **2014**, *4*, 4295–4298. [[CrossRef](#)]
37. Zhang, L.; Deng, B.; Li, N.; Zhong, H. Isomerization of Glucose into Fructose with Homogenous Amine-Type Base Catalysts: Amine Structure, Chain Length, and Kinetics. *Bioresour. Bioprocess.* **2019**, *6*, 35. [[CrossRef](#)]
38. Yue, C.; Rigutto, M.S.; Hensen, E.J.M. Glucose Dehydration to 5-Hydroxymethylfurfural by a Combination of a Basic Zirconosilicate and a Solid Acid. *Catal. Lett.* **2014**, *144*, 2121–2128. [[CrossRef](#)]
39. Nikolla, E.; Román-Leshkov, Y.; Moliner, M.; Davis, M.E. “One-Pot” Synthesis of 5-(Hydroxymethyl)Furfural from Carbohydrates Using Tin-Beta Zeolite. *ACS Catal.* **2011**, *1*, 408–410. [[CrossRef](#)]
40. Degirmenci, V.; Pidko, E.A.; Magusin, P.C.M.M.; Hensen, E.J.M. Towards a Selective Heterogeneous Catalyst for Glucose Dehydration to 5-Hydroxymethylfurfural in Water: CrCl₂ Catalysis in a Thin Immobilized Ionic Liquid Layer. *Chem. Cat. Chem.* **2011**, *3*, 969–972. [[CrossRef](#)]
41. Hayashi, S.; Hara, M.; Nakajima, K.; Baba, Y.; Noma, R.; Kitano, M.; Kondo, J.N.; Hayashi, S.; Hara, M. Nb₂O₅.NH₂O as a Heterogeneous Catalyst with Water-Tolerant Lewis Acid Sites. *J. Am. Chem. Soc.* **2011**, *133*, 4224–4227.
42. Watanabe, M.; Aizawa, Y.; Iida, T.; Aida, T.M.; Levy, C.; Sue, K.; Inomata, H. Glucose Reactions with Acid and Base Catalysts in Hot Compressed Water at 473 K. *Carbohydr. Res.* **2005**, *340*, 1925–1930. [[CrossRef](#)]

43. Qi, X.; Watanabe, M.; Aida, T.M.; Smith, R.L. Sulfated Zirconia as a Solid Acid Catalyst for the Dehydration of Fructose to 5-Hydroxymethylfurfural. *Catal. Commun.* **2009**, *10*, 1771–1775. [[CrossRef](#)]
44. Hou, Q.; Zhen, M.; Li, W.; Liu, L.; Liu, J.; Zhang, S.; Nie, Y.; Bai, C.; Bai, X.; Ju, M. Efficient Catalytic Conversion of Glucose into 5-Hydroxymethylfurfural by Aluminum Oxide in Ionic Liquid. *Appl. Catal. Environ.* **2019**, *253*, 1–10. [[CrossRef](#)]
45. Gallo, J.M.R.; Alonso, D.M.; Mellmer, M.A.; Dumesic, J.A. Production and Upgrading of 5-Hydroxymethylfurfural Using Heterogeneous Catalysts and Biomass-Derived Solvents. *Green Chem.* **2013**, *15*, 85–90. [[CrossRef](#)]
46. Zhang, W.; Zhu, Y.; Xu, H.; Gaborieau, M.; Huang, J.; Jiang, Y. Glucose Conversion to 5-Hydroxymethylfurfural on Zirconia: Tuning Surface Sites by Calcination Temperatures. *Catal. Today* **2020**, *351*, 133–140. [[CrossRef](#)]
47. Jiménez-Morales, I.; Santamaría-González, J.; Jiménez-López, A.; Maireles-Torres, P. Glucose Dehydration to 5-Hydroxymethylfurfural on Zirconium Containing Mesoporous MCM-41 Silica Catalysts. *Fuel* **2014**, *118*, 265–271. [[CrossRef](#)]
48. Atanda, L.; Silahua, A.; Mukundan, S.; Shrotri, A.; Torres-Torres, G.; Beltramini, J. Catalytic Behaviour of TiO₂-ZrO₂ Binary Oxide Synthesized by Sol-Gel Process for Glucose Conversion to 5-Hydroxymethylfurfural. *RSC Adv.* **2015**, *5*, 80346–80352. [[CrossRef](#)]
49. Gromov, N.V.; Taran, O.P.; Semeykina, V.S.; Danilova, I.G.; Pestunov, A.V.; Parkhomchuk, E.V.; Parmon, V.N. Solid Acidic NbO_x/ZrO₂ Catalysts for Transformation of Cellulose to Glucose and 5-Hydroxymethylfurfural in Pure Hot Water. *Catal. Lett.* **2017**, *147*, 1485–1495. [[CrossRef](#)]
50. Wang, Y.; Tong, X.; Yan, Y.; Xue, S.; Zhang, Y. Efficient and Selective Conversion of Hexose to 5-Hydroxymethylfurfural with Tin-Zirconium-Containing Heterogeneous Catalysts. *Catal. Commun.* **2014**, *50*, 38–43. [[CrossRef](#)]
51. Li, H.; Zhang, Q.; Liu, J.; Liu, X.; Chang, F.; Liu, Y.; Xue, W.; Yang, S. Selective Transformation of Carbohydrates into HMF Promoted by Carboxylic Acids Modified ZrMo Mixed Oxides. *Biomass Convers. Biorefinery* **2014**, *4*, 59–66. [[CrossRef](#)]
52. Zhou, Y.; Zhang, L.; Tao, S. Mesoporous ZrO₂ Nanopowder Catalysts for the Synthesis of 5-Hydroxymethylfurfural. *ACS Appl. Nano Mater.* **2019**, *2*, 5125–5131. [[CrossRef](#)]
53. Zhang, Y.; Xiong, Q.; Chen, Y.; Liu, M.; Jin, P.; Yan, Y.; Pan, J. Synthesis of Ceria and Sulfated Zirconia Catalysts Supported on Mesoporous SBA-15 toward Glucose Conversion to 5-Hydroxymethylfurfural in a Green Isopropanol-Mediated System. *Ind. Eng. Chem. Res.* **2018**, *57*, 1968–1979. [[CrossRef](#)]
54. Osatiashtiani, A.; Lee, A.F.; Granollers, M.; Brown, D.R.; Olivi, L.; Morales, G.; Melero, J.A.; Wilson, K. Hydrothermally Stable, Conformal, Sulfated Zirconia Monolayer Catalysts for Glucose Conversion to 5-HMF. *ACS Catal.* **2015**, *5*, 4345–4352. [[CrossRef](#)]
55. O'Dell, L.A.; Savin, S.L.P.; Chadwick, A.V.; Smith, M.E. A ²⁷Al MAS NMR Study of a Sol-Gel Produced Alumina: Identification of the NMR Parameters of the θ-Al₂O₃ Transition Alumina Phase. *Solid State Nucl. Magn. Reson.* **2007**, *31*, 169–173. [[CrossRef](#)]
56. Thommes, M.; Kaneko, K.; Neimark, A.V.; Olivier, J.P.; Rodriguez-Reinoso, F.; Rouquerol, J.; Sing, K.S.W. Physisorption of Gases, with Special Reference to the Evaluation of Surface Area and Pore Size Distribution (IUPAC Technical Report). *Pure Appl. Chem.* **2015**, *87*, 1051–1069. [[CrossRef](#)]
57. López-Asensio, R.; Cecilia, J.A.; Jiménez-Gómez, C.P.; García-Sancho, C.; Moreno-Tost, R.; Maireles-Torres, P. Selective Production of Furfuryl Alcohol from Furfural by Catalytic Transfer Hydrogenation over Commercial Aluminas. *Appl. Catal. Gen.* **2018**, *556*, 1–9. [[CrossRef](#)]
58. Klopogge, J.T.; Wood, B.J. Systematic XPS Study of Gallium-Substituted Boehmite. *J. Mater. Sci.* **2016**, *51*, 5436–5444. [[CrossRef](#)]
59. Klopogge, J.T.; Duong, L.V.; Wood, B.J.; Frost, R.L. XPS Study of the Major Minerals in Bauxite: Gibbsite, Bayerite and (Pseudo-)Boehmite. *J. Colloid Interface Sci.* **2006**, *296*, 572–576. [[CrossRef](#)] [[PubMed](#)]
60. Damyanova, S.; Grange, P.; Delmon, B. Surface Characterization of Zirconia-Coated Alumina and Silica Carriers. *J. Catal.* **1997**, *168*, 421–430. [[CrossRef](#)]
61. Guerrero-Urbaneja, P.; García-Sancho, C.; Moreno-Tost, R.; Mérida-Robles, J.; Santamaría-González, J.; Jiménez-López, A.; Maireles-Torres, P. Glycerol Valorization by Etherification to Polyglycerols by Using Metal Oxides Derived from MgFe Hydrotalcites. *Appl. Catal. Gen.* **2014**, *470*, 199–207. [[CrossRef](#)]

62. Reddy, B.M.; Sreekanth, P.M.; Yamada, Y.; Kobayashi, T. Surface Characterization and Catalytic Activity of Sulfate-, Molybdate- and Tungstate-Promoted Al₂O₃-ZrO₂ Solid Acid Catalysts. *J. Mol. Catal. Chem.* **2005**, *227*, 81–89. [[CrossRef](#)]
63. Smith, M.E. Application of 27Al NMR Techniques to Structure Determination in Solids. *Appl. Magn. Reson* **1993**, *4*, 1–64. [[CrossRef](#)]
64. Hill, M.R.; Bastow, T.J.; Celotto, S.; Hill, A.J. Integrated Study of the Calcination Cycle from Gibbsite to Corundum. *Chem. Mater.* **2007**, *19*, 2877–2883. [[CrossRef](#)]
65. Chagas, L.H.; de Carvalho, G.S.G.; San Gil, R.A.S.; Chiaro, S.S.X.; Leitão, A.A.; Diniz, R. Obtaining Aluminas from the Thermal Decomposition of Their Different Precursors: An ²⁷Al MAS NMR and X-Ray Powder Diffraction Studies. *Mater. Res. Bull.* **2014**, *49*, 216–222. [[CrossRef](#)]
66. Kwak, J.H.; Hu, J.Z.; Kim, D.H.; Szanyi, J.; Peden, C.H.F. Penta-Coordinated Al³⁺ Ions as Preferential Nucleation Sites for BaO on γ-Al₂O₃: An Ultra-High-Magnetic Field ²⁷Al MAS NMR Study. *J. Catal.* **2007**, *251*, 189–194. [[CrossRef](#)]
67. Tomaszewska, J.; Bieliński, D.; Binczarski, M.; Berłowska, J.; Dziugan, P.; Piotrowski, J.; Stanishevsky, A.; Witońska, I.A. Products of Sugar Beet Processing as Raw Materials for Chemicals and Biodegradable Polymers. *RSC Adv.* **2018**, *8*, 3161–3177. [[CrossRef](#)]
68. Ranoux, A.; Djanashvili, K.; Arends, I.W.C.E.; Hanefeld, U. 5-Hydroxymethylfurfural Synthesis from Hexoses Is Autocatalytic. *ACS Catal.* **2013**, *3*, 760–763. [[CrossRef](#)]
69. Portillo Perez, G.; Mukherjee, A.; Dumont, M.J. Insights into HMF Catalysis. *J. Ind. Eng. Chem.* **2019**, *70*, 1–34. [[CrossRef](#)]
70. Yan, L.; Ma, R.; Wei, H.; Li, L.; Zou, B.; Xu, Y. Ruthenium Trichloride Catalyzed Conversion of Cellulose into 5-Hydroxymethylfurfural in Biphasic System. *Bioresour. Tech.* **2019**, *279*, 84–91. [[CrossRef](#)]
71. Prat, D.; Wells, A.; Hayler, J.; Sneddon, H.; McElroy, C.R.; Abou-Shehadeh, S.; Dunn, P.J. CHEM21 Selection Guide of Classical- and Less Classical-Solvents. *Green Chem.* **2015**, *18*, 288–296. [[CrossRef](#)]
72. Combs, E.; Cinlar, B.; Pagan-Torres, Y.; Dumesic, J.A.; Shanks, B.H. Influence of Alkali and Alkaline Earth Metal Salts on Glucose Conversion to 5-Hydroxymethylfurfural in an Aqueous System. *Catal. Commun.* **2013**, *30*, 1–4. [[CrossRef](#)]
73. Stošić, D.; Bennici, S.; Pavlović, V.; Rakić, V.; Auroux, A. Tuning the Acidity of Niobia: Characterization and Catalytic Activity of Nb₂O₅-MeO₂ (Me = Ti, Zr, Ce) Mesoporous Mixed Oxides. *Mater. Chem. Phys.* **2014**, *146*, 337–345. [[CrossRef](#)]
74. Córdova-Pérez, G.E.; Torres-Torres, G.; Ortíz-Chi, F.; Godavarthi, S.; Silahua-Pavón, A.A.; Izquierdo-Colorado, A.; da Costa, P.; Hernández-Como, N.; Aleman, M.; Espinosa-González, C.G. Effect of Acid-Basic Sites Ratio on the Catalytic Activity to Obtain 5-HMF from Glucose Using Al₂O₃-TiO₂-W Catalysts. *Chem. Sel.* **2018**, *3*, 12854–12864. [[CrossRef](#)]
75. Gao, Y.; Wang, X.; Yang, H.; Chen, H. Characterization of products from hydrothermal treatments of cellulose. *Energy* **2012**, *42*, 457–465. [[CrossRef](#)]
76. He, J.; Li, H.; Riisager, A.; Yang, S. Catalytic Transfer Hydrogenation of Furfural to Furfuryl Alcohol with Recyclable Al-Zr@Fe Mixed Oxides. *Chem. Cat. Chem.* **2018**, *10*, 430–438. [[CrossRef](#)]

